



# Effect of Sc and Zr on recrystallization behavior of 7075 aluminum alloy

Jin-feng LENG<sup>1</sup>, Bing-hui REN<sup>1</sup>, Qing-bo ZHOU<sup>2</sup>, Ji-wei ZHAO<sup>1</sup>

1. School of Materials Science and Engineering, University of Ji'nan, Ji'nan 250022, China;

2. Shandong Zhonglv Carbon Material Co., Ltd., Ji'nan 250031, China

Received 27 November 2020; accepted 10 May 2021

**Abstract:** The static recrystallization behavior of 7075 aluminum alloy containing  $Al_3(Sc,Zr)$  phase prepared by casting and the relationship between recrystallization behavior and mechanical properties were studied. The addition of Sc and Zr made the Sc–Zr–7075 aluminum alloy remain the most of fibrous structure and high-density dislocations formed in the extrusion process, resulting in the recrystallization fraction of the alloy decreasing from 35% to 22%, and the corresponding fraction of substructure increasing from 59% to 67%. The Sc and Zr effectively inhibited the recrystallization behavior of 7075 aluminum alloy mainly, which was attributed to the fact that the existence of fine and coherent  $Al_3(Sc,Zr)$  phase ( $r=35$  nm,  $f=1.8\times 10^{-3}$ ) strongly pinned the dislocations and grain boundaries, preventing the dislocations from rearranging into sub-grain boundaries and from developing into high angle grain boundaries, and further hindering the formation and growth of recrystallized core of the alloy.

**Key words:** 7075 aluminum alloy;  $Al_3(Sc,Zr)$  phase; recrystallization; mechanical properties

## 1 Introduction

7075 aluminum alloys have been widely applied in the aerospace and automobile manufacturing industries due to their high specific strength and fracture toughness [1–3]. In the subsequent heating process of the 7075 aluminum alloy after plastic deformation, the structure of the 7075 aluminum alloy undergoes recovery, recrystallization, and grain growth [4,5]. The degrees of deformation, recrystallization annealing temperature, original grain size, and the types of alloying elements can greatly affect the recrystallization grain structures of alloy. For example, most of the grain morphology in the 7050 alloys maintains the original shape without recrystallization when the hot rolling deformation is less than 20% [6]. The dynamic recrystallization process with the homogenized annealed initial microstructure is slower than the dynamic

recrystallization process with the extruded initial microstructure [7]. With the gradual increase in the annealing temperature from 250 to 500 °C, the structure of the 7150 alloys gradually changes from the recovery structure to the fully recrystallized structure [8]. However, the addition of alloying elements promotes or inhibits the static recrystallization process of 7075 aluminum alloy, and these two mechanisms compete with each other [9,10].

The effects of alloying elements on the static recrystallization process of 7075 aluminum alloy mainly depend on the size, volume fraction, and distribution of the second phase that is formed due to the addition of alloying elements [11–13]. The coarse second phases ( $Al_2CuMg$ ,  $(Mg,Cu,Al)Zn_2$ ,  $Mg_{32}(Al,Cu,Zn)_{49}$ ,  $\alpha-Al(Mn,Fe,Si)$  phases, etc.,  $>1$   $\mu m$ ) formed during the solidification process can promote the static recrystallization of the alloy [14,15]. The fine dispersed second phases ( $Al_3(Sc,Zr)$ ,  $(Al,Cr)_3Zr$ , etc.,  $<1$   $\mu m$ ) precipitated

during homogenization and subsequent heat treatment have a strong inhibitory effect on the nucleation and growth of the static recrystallization of alloy [16]. For example, the AA1200 and AA8006 aluminum alloys containing coarse second phase (the size  $\geq 1 \mu\text{m}$ ) undergo discontinuous or continuous recrystallization during the annealing process [17]. Moreover, the Al(Cr,Mn,Fe)Si and (Al,Si)<sub>3</sub>Zr dispersions significantly improve the recrystallization resistance of 6082 aluminum alloy [18].

Sc and Zr have been recognized as effective microalloying elements in structural aircraft aluminum materials. The formation of primary Al<sub>3</sub>(Sc,Zr) particles provides effective nucleation sites in the solidification process, which results in significant grain refinement [19]. The secondary Al<sub>3</sub>(Sc,Zr) phases with the size of 2–100 nm precipitate in the homogenization and the subsequent heat treatment. This not only plays a role in the Orowan strengthening by secondary Al<sub>3</sub>(Sc,Zr) phase [20–22] but also enhances the recrystallization resistance of the alloy during the plastic deformation and subsequent heat treatment process [23–25]. The Al–5.4Zn–2.0Mg–0.35Cu–0.32Mn alloy without Sc and Zr additions is completely recrystallized after the heat treatment process, while the alloy containing 0.25% Sc and 0.1% Zr does not recrystallize and retains the fibrous grain structure [26]. For the cold deformed Al–Zn–Mg–Cu alloy without the addition of Sc and Zr, local recrystallization occurs after annealing at 450 °C for 0.5 h. However, the cold deformed Al–Zn–Mg–Cu–Sc–Zr alloy with the addition of Sc and Zr does not recrystallize even after annealing at 450 °C for 10 h [27]. Moreover, the addition of Sc and Zr can stabilize the grain size of the hot deformed Al–Zn–Mg–Cu alloy. After annealing at 350 °C for 10 h and at 450 °C for 10 h, the grain size of the hot deformed Al–Zn–Mg–Cu–Sc–Zr alloy does not change [28]. Furthermore, Al<sub>3</sub>(Sc,Zr) phase remains fine at high temperatures without coarsening, which significantly increases the recrystallization temperature of the alloy. This is mainly because the diffusion rate of Zr atoms is lower than that of Sc atoms at the same temperature. The Al<sub>3</sub>(Sc,Zr) phase with Sc atoms is formed as cores while the phase with Zr atoms is formed as shells during the homogenization and subsequent heat treatment process [29]. Extensive research

work has been conducted on the strengthening and toughening mechanism of Sc–Zr–7075 alloy as well as the precipitation characteristics of the Al<sub>3</sub>(Sc,Zr) phase [30–32]. However, the mechanism of the precipitation of the Al<sub>3</sub>(Sc,Zr) phase on the static recrystallization of the plastically deformed 7075 aluminum alloy during the subsequent healing process has less been systematically studied.

In this work, the influence of the Al<sub>3</sub>(Sc,Zr) phase on the static recrystallization process of 7075 aluminum alloy was studied in detail by electron backscattered diffractometry (EBSD) and transmission electron microscopy (TEM). The mechanism of the second phase on the migration resistance and speed of grain boundaries in 7075 aluminum alloy was qualitatively described, and the relationship between static recrystallization behavior and mechanical properties was further clarified.

## 2 Experimental

Al, Zn, Mg (>99.9 wt.% in purity), Al–50%Cu, Al–4%Ti, Al–5%Zr and Al–2%Sc master alloys were used as raw alloys. The nominal composition of 7075 aluminum alloys without (7075) and with Sc and Zr (Sc–Zr–7075) is listed in Table 1. The total mass of the ingots was 5500 g.

**Table 1** Nominal compositions of alloys used in present work (wt.%)

Alloy	Zn	Mg	Cu	Ti	Sc	Zr	Fe	Si	Al
7075	5.6	2.5	1.6	0.05	–	–	<0.1	<0.1	Bal.
Sc–Zr–7075	5.6	2.5	1.6	0.05	0.1	0.1	<0.1	<0.1	Bal.

The 7075 and Sc–Zr–7075 alloys were prepared by conventional casting methods. Pure aluminum ingots were put into the graphite crucible preheated to 300 °C and heated to 730 °C. Then, master alloys were added to the molten aluminum solution. The master alloys were stirred and declared after they were completely melted. Finally, the melts were poured into a metal mold (size:  $d90 \text{ mm} \times 300 \text{ mm}$ ) preheated to 200 °C at an appropriate rate. After removing the head and tail, the as-cast ingots were subjected to single-stage (465 °C, 16 h) homogenization (The choice of temperature is similar to the Ref. [27]). All the

homogenized ingots were cooled down to 200 °C in a furnace and then air cooled down to room temperature. Then, the ingot was extruded, and the extruded rods were subject to the solution and then aging heat treatment (120 °C, 24 h) (T6).

The microstructure of 7075 aluminum alloys was studied by the optical microscopy (OM), electron backscattered diffractometry (EBSD), transmission electron microscopy (TEM), and high-resolution electron microscopy (HRTEM). The properties of 7075 aluminum alloys were studied through hardness measurements and tensile tests. The hardness of alloys was measured using a Brinell hardness tester of HBRVU–187.5 under a load of 1839 N and a loading time of 30 s. At least ten points were measured for each sample ( $d22 \text{ mm} \times 5 \text{ mm}$ ). Tensile tests were conducted with a WDG–1060 electronic universal testing machine with a loading speed of 2 mm/min (GB/T 228–2002). The morphology of the samples was observed through scanning electron microscopy (SEM) with an FEI-QUANTA FEG250 instrument and TEM with a JEM–2010 transmission electron microscope. The samples for TEM analysis were prepared by cutting a 500  $\mu\text{m}$  section from the center of the samples through wire cutting, rough grinding to below 300  $\mu\text{m}$ , and finally fine grinding to about 100  $\mu\text{m}$ . The foils were prepared by twin-jet electropolishing and the thinned sections were analyzed in bright and dark fields and high-resolution TEM. To evaluate the recrystallized structures and quantify the recrystallization fraction, all deformed samples after solution treatment were sectioned parallel to the compression axis along the direction of the centerline and then examined with EBSD. The step size was 0.5  $\mu\text{m}$ , and the EBSD data were analyzed using TSL OIM software.

### 3 Results and discussion

#### 3.1 Microstructure and hardness after solution treatment

To determine the best solution temperature of 7075 aluminum alloy, the hardness and microstructure of 7075 aluminum alloy were analyzed. The hardness values of 7075 and Sc–Zr–7075 aluminum alloy processed at different temperatures for 2 h are shown in Fig. 1. When the solution temperature was lower than 470 °C, the hardness of the two alloys increased with the

increase in the solution temperature. Since alloys maintained a fibrous structure, the growth of sub-grain was not obvious. The second phase of alloy gradually dissolved into the Al matrix with the increase in temperature, and solid solution strengthening played a dominating role. The hardness of 7075 alloys showed an obvious decreasing trend when it was a solid solution at 480 °C. The dissolution of the low melting point eutectic phase was completed, and the sub-grain growth was very obvious. At the same time, part of the alloy was recrystallized, and this weakened the effect of solid solution strengthening on the alloy.

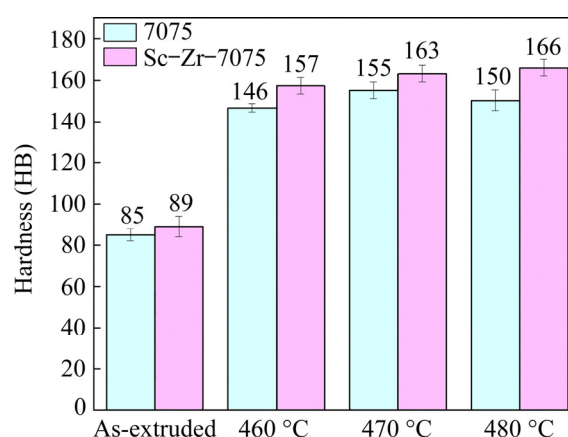
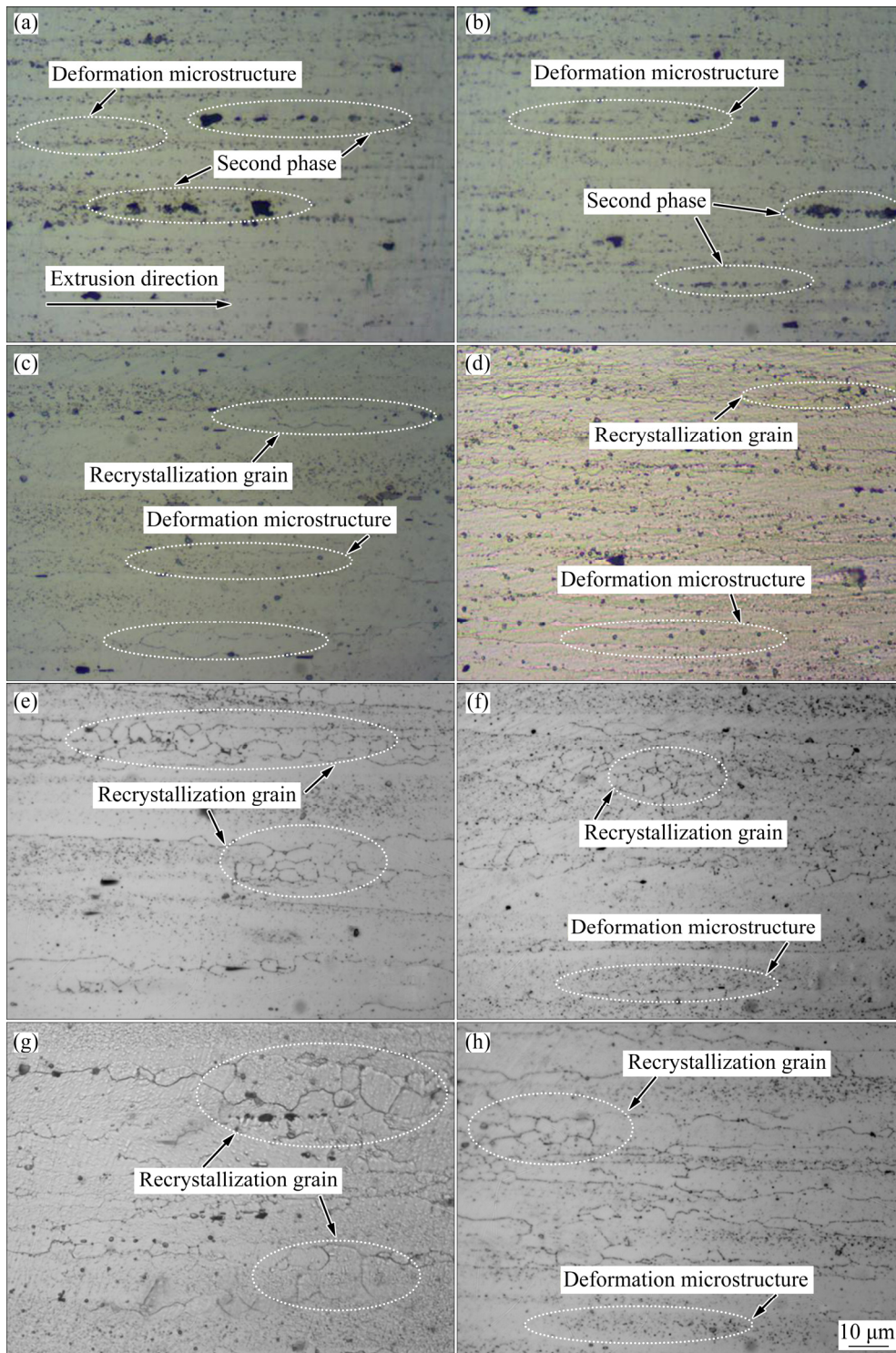


Fig. 1 Hardness values of 7075 and Sc–Zr–7075 aluminum alloys treated at different temperatures for 2 h

On the contrary, the hardness of Sc–Zr–7075 alloy was still in the rising stage, but the degree of improvement was slightly reduced. This is mainly attributed to the fact that the alloy maintained the deformation recovery structure, and the increase in grain size was not obvious. With the increase in temperature, the second phase gradually dissolved into the matrix, and solid solution strengthening still played an important role. Therefore, the hardness of Sc–Zr–7075 aluminum alloy gradually increased with the increase in the solid solution temperature.

The optical images of 7075 and Sc–Zr–7075 aluminum alloys after solid solution treatment at different temperatures for 2 h are shown in Fig. 2. The original grains of 7075 and Sc–Zr–7075 alloys are elongated along the extrusion direction after hot extrusion deformation. These grains were confirmed to have typical fibrous structures. Also, the second phase of the alloy was broken and distributed in chains along the extrusion direction.



**Fig. 2** Optical images of 7075 (a, c, e, g) and Sc-Zr-7075 (b, d, f, h) aluminum alloys processed at different temperatures for 2 h: (a, b) As-extruded; (c, d) 460 °C; (e, f) 470; (g, h) 480 °C

The second phase of the Sc-Zr-7075 alloy was finer and more evenly distributed compared to that of the 7075 alloys (Figs. 2(a, b)). After the solid-solution treatment at 460 °C for 2 h, the fine second phase in 7075 alloy re-dissolved, and the large size of the second phase gradually dissolved. The

recrystallized grains began to appear, but they still maintained the extruded fibrous structure of the alloy (Fig. 2(c)). The Sc-Zr-7075 alloy remained a completely unrecrystallized fibrous structure, and only a smaller second phase was present in the alloy (Fig. 2(d)). After the solid solution treatment at

470 °C for 2 h, the number of sub-grains of 7075 aluminum alloy began to increase, and the recrystallization fraction increased. However, the Sc–Zr–7075 alloy showed recrystallized grains in a few regions.

Although the second phase of 7075 and Sc–Zr–7075 alloy completely re-dissolved after a solid solution treatment at 480 °C for 2 h, the recrystallized grains of the alloy began to merge and grow. The Sc–Zr–7075 alloy had a smaller degree of grain growth compared to the 7075 alloys. This indicates that the co-addition of Sc and Zr to 7075 alloy significantly improved the recrystallization resistance, and the alloy still kept most of the fine sub-grain structure at higher temperatures. Therefore, the addition of Sc and Zr significantly increased the recrystallization temperature of 7075 alloy [33]. By combining the microstructure and hardness of 7075 and Sc–Zr–7075 aluminum alloys, the best solid solution treatment process was 470 °C, 2 h.

### 3.2 Recrystallization microstructure

To further study the influence of Sc and Zr addition on the recrystallization process of alloy, the microstructure of 7075 and Sc–Zr–7075 aluminum alloys after the optimal process (470 °C, 2 h) was analyzed by EBSD. The EBSD pole images of 7075 and Sc–Zr–7075 aluminum alloys after treatment at 470 °C for 2 h are demonstrated in Fig. 3. The 7075 and Sc–Zr–7075 aluminum alloys still maintained the slender fiber structure in the extruded shape, and some recrystallized grains were found in the fiber structure. The fibrous structure of the alloy had a corresponding preferred orientation, with [101] and [111] orientations as the main ones, and the original orientation of the extruded structure

was still present. The orientation of the recrystallized grain was dominated by the [001] orientation. This is because a large number of dislocations were stored in the [001] orientation grains, and the driving force for recrystallization was relatively high. The [001] orientation grain was preferentially recrystallized, so a large number of recrystallized grains appeared in this region. The fiber structure of Sc–Zr–7075 alloy was finer, and only a few uniform and fine recrystallized grains appeared. This is mainly due to the addition of Sc and Zr to form the  $\text{Al}_3(\text{Sc,Zr})$  phase that was coherent with the aluminum matrix. The  $\text{Al}_3(\text{Sc,Zr})$  phase hindered the movement of dislocations and increased the local dislocation density, thereby promoting the formation of deformation structure in the Sc–Zr–7075 alloy during the extrusion process (Fig. 4).

The grain morphology and boundary distribution of the 7075 and Sc–Zr–7075 aluminum alloys after the treatment at 470 °C for 2 h are presented in Fig. 5. The grain morphology showed the distribution of deformed structure, substructure, and recrystallized structure. The distribution of these structures was determined using OIM software. It can be seen from Figs. 5(a, b) that parts of the grains were elongated along the extrusion direction, and the deformed grains were distributed with substructures composed of low-angle grain boundaries. Meanwhile, some recrystallized grains formed by high-angle grain boundaries could also be observed. The quantitative analysis results of deformed structure, substructure, and recrystallized structure are shown in Figs. 5(c, d). Compared with 7075 alloys, the addition of Sc and Zr reduced the recrystallization fraction of Sc–Zr–7075 alloy from 35% to 22%, and the substructure fraction increased

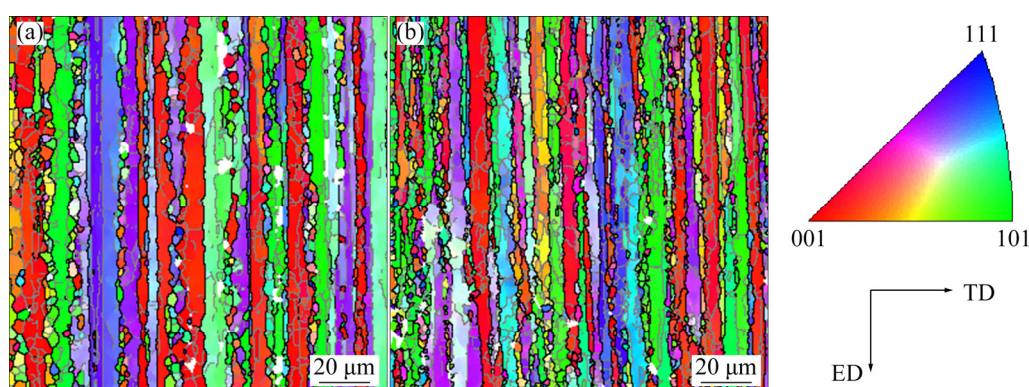


**Fig. 3** Inverse pole figures (IPF) of 7075 (a) and Sc–Zr–7075 (b) aluminum alloys after treatment at 470 °C for 2 h

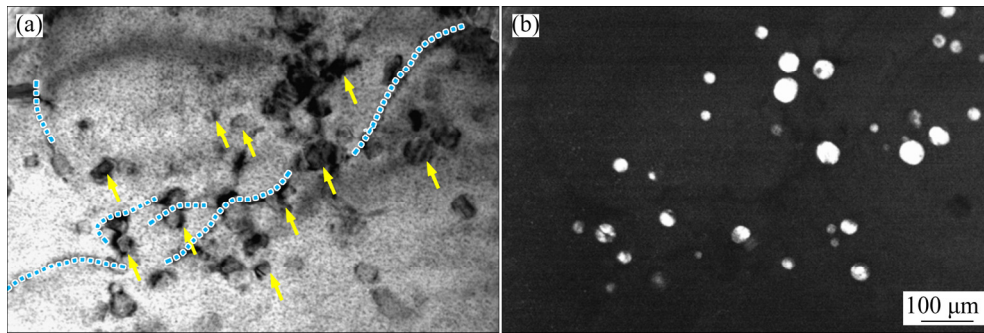


**Fig. 4** TEM images of  $\text{Al}_3(\text{Sc,Zr})$  phase (T6): (a) Bright-field; (b) Dark-field

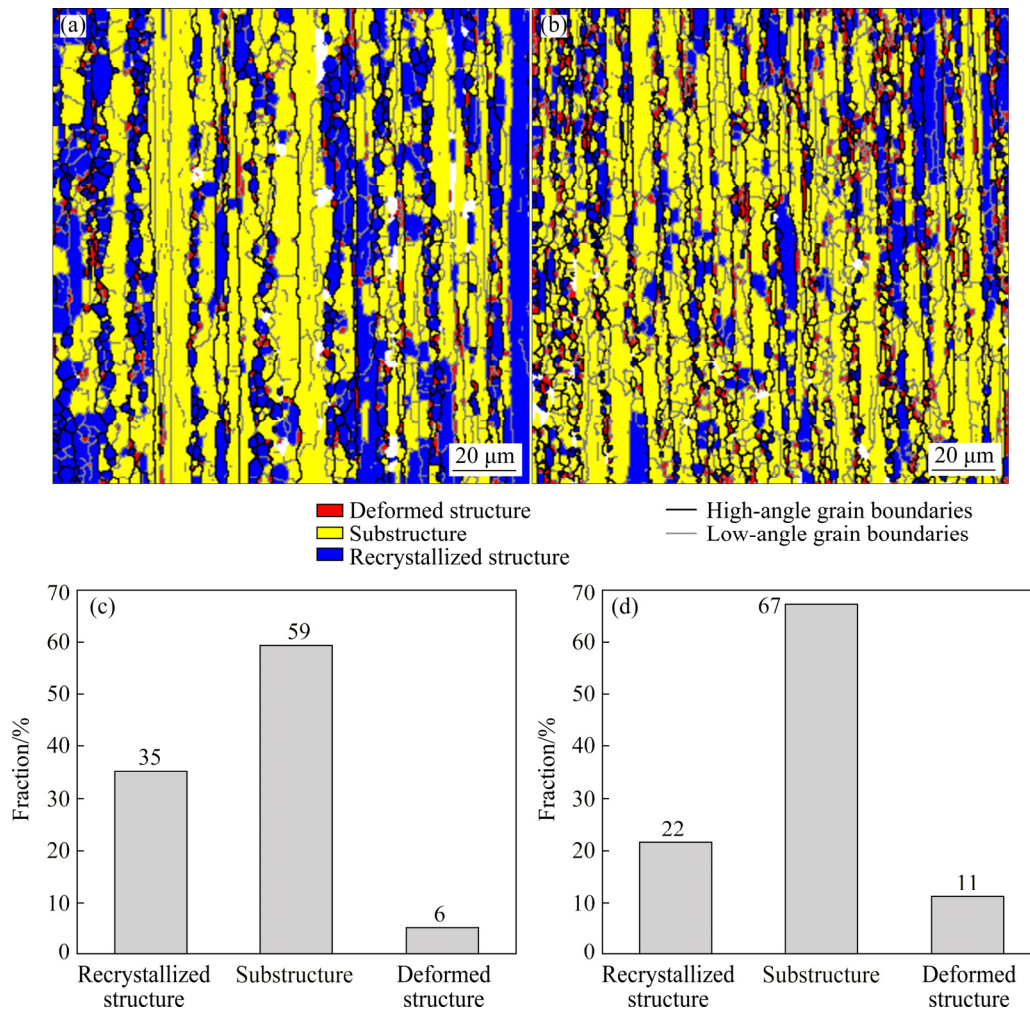


**Fig. 5** Grain morphologies (a, b) and grain boundary distributions (c, d) of 7075 and Sc-Zr-7075 aluminum alloys after treatment at 470 °C for 2 h: (a, c) 7075; (b, d) Sc-Zr-7075

from 59% to 67%. Moreover, the recrystallized grains of Sc-Zr-7075 alloy were finer equiaxed. This is mainly attributed to the nano-sized  $\text{Al}_3(\text{Sc,Zr})$  phase that can effectively hinder the migration of grain boundaries and the formation of sub-grain structure [34]. The statistical results (Fig. 6) show that the proportions of low-angle grain boundaries increased from 61% of 7075 to 78% of Sc-Zr-7075 alloys, and the corresponding

proportions of high-angle grain boundaries decreased from 39% to 22%.

### 3.3 Kernel average misorientation (KAM) analysis

The KAM value represents the average orientation angle of a given point relative to all its neighbors, and it is used to describe the local dislocation density distribution [35]. Figure 7 shows

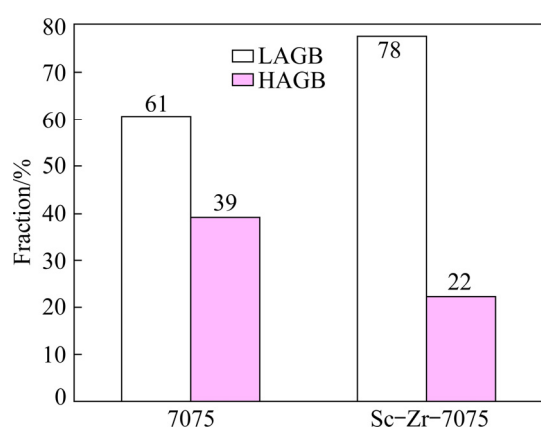


**Fig. 6** High-angle grain boundary (HAGB) and low-angle grain boundary (LAGB) distributions of 7075 and Sc-Zr-7075 aluminum alloys after treatment at 470 °C for 2 h

the KAM images of 7075 and Sc-Zr-7075 aluminum alloys after the treatment at 470 °C for 2 h. The Sc-Zr-7075 alloy still maintained a high dislocation density after treatment at 470 °C for 2 h. This indicates that the driving force (lattice distortion energy) required for conversion to recrystallization was low and the degree of recrystallization was smaller compared to 7075 aluminum alloy. The results are consistent with Fig. 5. Furthermore, the type of grain boundary at the high KAM value (high-density dislocation) area is low angle grain boundaries. This is mainly due to the  $\text{Al}_3(\text{Sc,Zr})$  phase strongly pinning the dislocations of the alloy. Consequently, the sub-grain boundaries did not effectively absorb the dislocations and still maintained low-angle grain boundaries to inhibit the recrystallization nucleation of the alloy.

### 3.4 Recrystallization mechanism

To more clearly and intuitively study the influence of the second phase on the recrystallization process of alloy, the microstructure of 7075 and Sc-Zr-7075 aluminum alloys (T6) was analyzed by TEM. TEM images of 7075 aluminum alloy are demonstrated in Fig. 8. There are small amounts of rod-shaped (0.3–0.6  $\mu\text{m}$ ) and spherical (0.1–0.3  $\mu\text{m}$ ) precipitated phases in the alloy. The recrystallized nuclei occurred in the deformation zone around these precipitated phases (Fig. 8(a)). As shown in Fig. 8(b), Region A contained a large number of dislocations. This suggests that this part of the region has also undergone the recovery and it still retained the characteristics of the deformed grains. The dislocation lines inside the sub-grain represented by Region B have disappeared, but the light and dark stripes appeared. This indicated that the strain distribution in this area was uneven. The grain has undergone a relatively sufficient recovery and gradually transformed into the recrystallized grain.

On the contrary, there was no dislocation line inside the adjacent Region C, and the contrast was uniform. At the same time, adjacent grain constituted a standard triangular grain boundary, and the grain boundary was relatively straight. The angle between adjacent grain boundaries was approximately 120°. Therefore, it was confirmed that the grain was a distortion-free recrystallized grain. Besides, the recrystallization of 7075 aluminum alloy was relatively complete, as shown in Figs. 8(c, d). This was consistent with the EBSD results of Figs. 5 and 6. This is mainly due to the weak ability of the  $\text{Al}_2\text{CuMg}$  phase (average size of

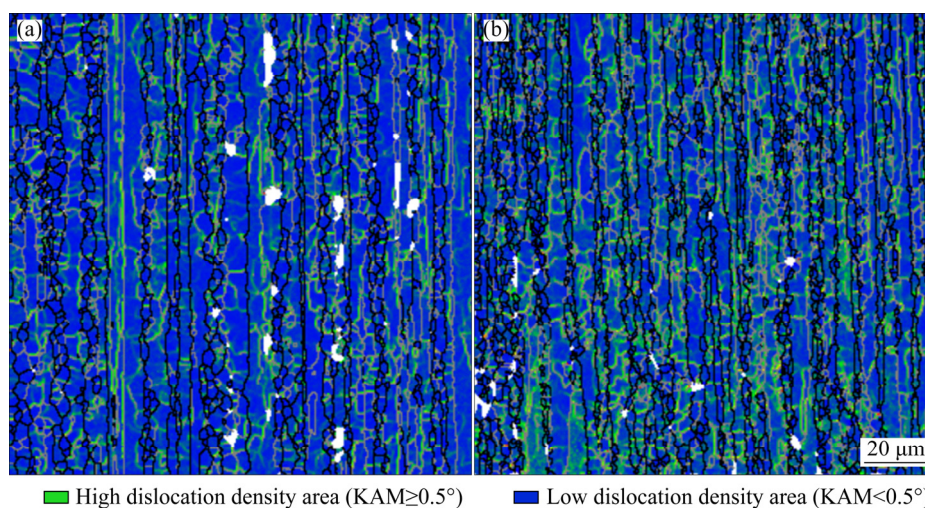
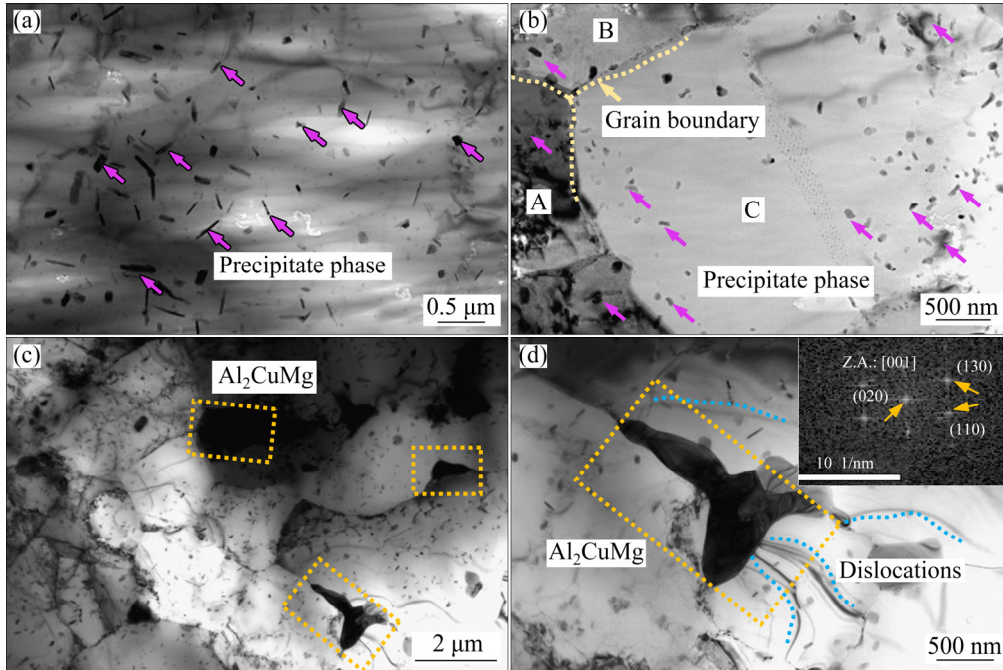


**Fig. 7** KAM images of 7075 (a) and Sc-Zr-7075 (b) aluminum alloy after treatment at 470 °C for 2 h

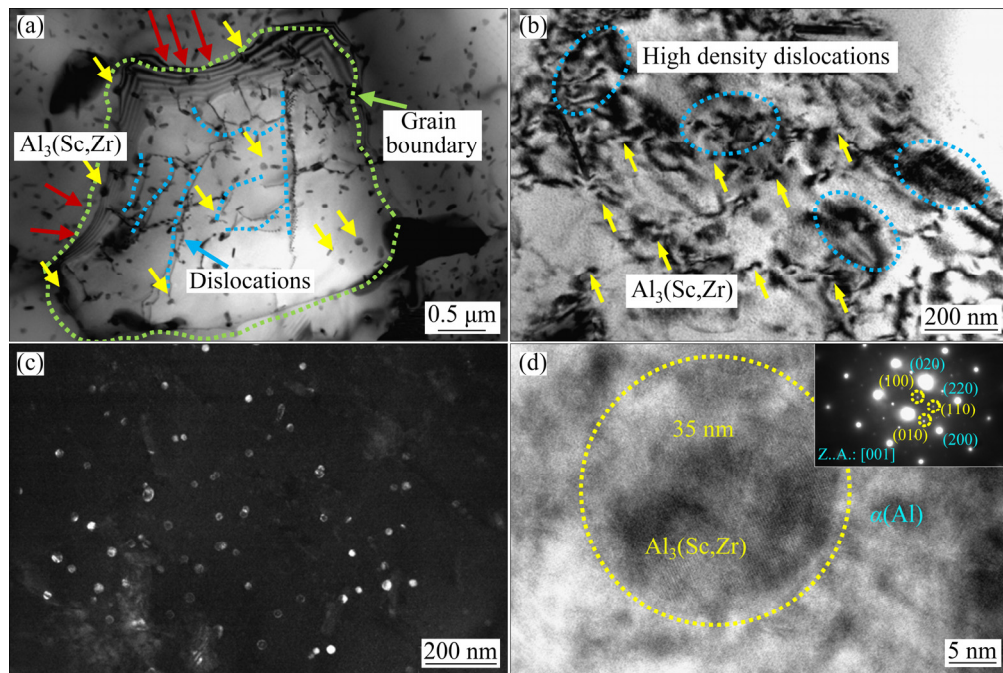
1.9  $\mu\text{m}$ ) that hindered the migration of dislocations. The sub-grain boundary absorbing dislocations gradually evolved into high-angle grain boundaries to promote the recrystallization of the alloy.

Figure 9 shows the TEM images of Sc–Zr–7075 aluminum alloy (T6). High-density dislocation

entanglement was still maintained in the grains (as shown by the blue circle), and the dislocations were arranged randomly without obvious regularity. The contrast of the high-strain region where the dislocations were enriched was still relatively high (Fig. 9(b)). From Fig. 9(c), it can be seen that the



**Fig. 8** TEM images of 7075 aluminum alloy (T6): (a, b) Precipitated phase and its interaction with dislocations and grain boundaries; (c, d)  $\text{Al}_2\text{CuMg}$  phase and its interaction with dislocations



**Fig. 9** TEM images of Sc–Zr–7075 aluminum alloy (T6): (a, b)  $\text{Al}_3(\text{Sc,Zr})$  phase and its interaction with dislocations; (c) Dark field image of  $\text{Al}_3(\text{Sc,Zr})$  phase; (d) HRTEM of  $\text{Al}_3(\text{Sc,Zr})$  phase

$\text{Al}_3(\text{Sc,Zr})$  phase (as shown by the yellow arrow) was evenly dispersed in the aluminum matrix. Statistics results indicate that the average size of the  $\text{Al}_3(\text{Sc,Zr})$  phase was 35 nm. Moreover, the  $\text{Al}_3(\text{Sc,Zr})$  phase and  $\alpha(\text{Al})$  maintained a coherent relationship, as shown in Fig. 9(d). From Fig. 9(a), it is observed that there were fine dispersed  $\text{Al}_3(\text{Sc,Zr})$  phases and a large number of dislocations in the alloy.

Besides, the spherical  $\text{Al}_3(\text{Sc,Zr})$  phase was distributed near the dislocation lines and sub-grain boundaries, and the dislocation lines surrounded the  $\text{Al}_3(\text{Sc,Zr})$  phase. The recrystallization process of Sc–Zr–7075 aluminum alloy was significantly suppressed compared to that of 7075 aluminum alloy. This was mainly due to the small and coherent  $\text{Al}_3(\text{Sc,Zr})$  phase that strongly hindered the dislocations and grain boundaries, preventing the dislocations from rearranging into sub-grain boundaries and from developing into LAGBs. This further inhibited the recrystallization nucleation.

Furthermore, part of the grain boundaries of the undistorted grains was bowed to the side of the sub-crystal containing dislocations (as shown by the red arrow in Fig. 9(a)). The contrast of sub-grain regions tends to be consistent with that of the undistorted grains, and the interface between the two types of subcrystalline grains was gradually blurred. These results indicate that the undistorted recrystallized core was deepened toward the side

containing dislocation sub-grain, and the core gradually annexed the sub-grain and grew up. Thus, it is confirmed that the recrystallization nucleation mechanism of Sc–Zr–7075 aluminum alloy is the protrusion nucleation of the grain boundary.

A schematic diagram of the influence of the nano-size  $\text{Al}_3(\text{Sc,Zr})$  phase on the recrystallization mechanism of 7075 aluminum alloy is shown in Fig. 10. For 7075 aluminum alloy, the dislocation density within the grain is relatively low. Moreover, the  $\text{Al}_2\text{CuMg}$  phase (with a size of 1.9  $\mu\text{m}$ ) in the alloy cannot effectively suppress the dislocation movement. As a result, the sub-grain boundaries continuously absorbed dislocations and gradually evolved into large-angle grain boundaries to promote the recrystallization process of the alloy, as shown in Fig. 8. Compared with 7075 aluminum alloy, Sc–Zr–7075 aluminum alloy had a smaller degree of recrystallization. This is mainly due to the small and coherent  $\text{Al}_3(\text{Sc,Zr})$  phase in the Sc–Zr–7075 aluminum alloy that strongly inhibited the dislocations and grain boundaries, preventing the dislocations from rearranging into sub-grain boundaries and from developing into large angles. This further hindered the recrystallization nucleation and the growth of the alloy recrystallization core, as shown in Figs. 9(a, c). Besides, since the diffusion rate of Sc atoms was larger than that of Zr atoms at the same temperature, the  $\text{Al}_3(\text{Sc,Zr})$  phase with Sc atoms was formed as

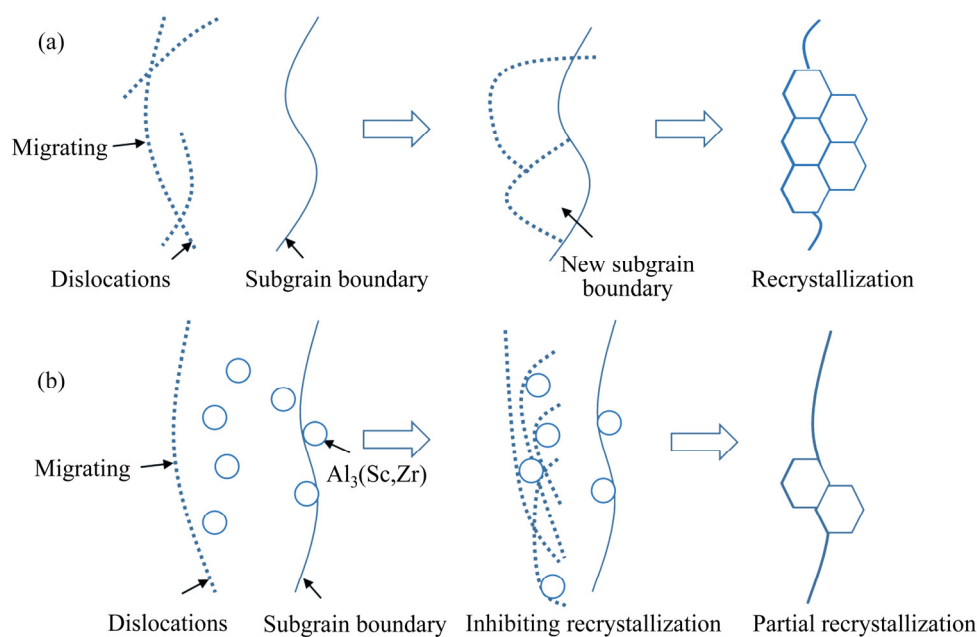


**Fig. 10** Schematic diagram of influence of nano-size  $\text{Al}_3(\text{Sc,Zr})$  phase on recrystallization mechanism of 7075 (a) and Sc–Zr–7075 (b) aluminum alloy

cores while the phase with Zr atoms was formed as shells. The  $\text{Al}_3(\text{Sc,Zr})$  phase remained fine without coarsening at high temperatures, which increased the recrystallization temperature of the alloy significantly.

The effect of the second phase on the static recrystallization of 7075 aluminum alloy is either promotion or inhibition, depending on the volume fraction and particle size of the second phase in the matrix. When the distance  $\lambda$  and the particle size  $d$  of the second phase particles are both large ( $\lambda \geq 1 \mu\text{m}$ ,  $d \geq 0.3 \mu\text{m}$ ), the second phase particles can promote the recrystallization process. On the contrary, the second phase particles with smaller sizes ( $\lambda < 1 \mu\text{m}$ ,  $d < 0.3 \mu\text{m}$ ) have an inhibitory effect on the recrystallization process. This is mainly because the precipitated phase distributing inside the grain and at the grain boundaries hinders the migration of grain boundaries and dislocations through Zener pinning, thereby inhibiting the recrystallization of the alloy. The force of the second phase hindering the migration of grain boundaries or dislocations can be expressed by [36]

$$P_Z = k\gamma \left( \frac{f}{r} \right) \quad (1)$$

where  $P_Z$  represents the pinning force of the relative migration of grain boundary or dislocation;  $f$  represents the volume fraction of the second phase;  $r$  represents the radius of the second phase;  $\gamma$  represents the interface energy of the pinned grain boundary or dislocation. The interface energy is a constant for aluminum alloy. It can be seen that the larger the volume fraction of the second phase and the smaller the radius, the more significant the resistance of the second phase to grain boundary or dislocation migration.

In this work, the average radius of the  $\text{Al}_3(\text{Sc,Zr})$  phase was about 35 nm, the volume fraction was  $1.8 \times 10^{-3}$ , and the fine phase was well dispersed in the aluminum matrix. According to the Zener theory, the fine and well-dispersed  $\text{Al}_3(\text{Sc,Zr})$  phase has a strong inhibiting effect on dislocations and subgrain boundaries. As such, the cellular structure in the cold-deformed structure was fuzzy and the dislocation entangled significantly. Furthermore, the dislocation rearrangement into sub-grain boundaries and the progress of sub-grain growth were hindered during the heat treatment, and the formation of recrystallized nuclei was

delayed. During the growth of recrystallized nuclei, the fine  $\text{Al}_3(\text{Sc,Zr})$  phase hindered the migration of large-angle grain boundaries, inhibiting the growth of recrystallized cores and preventing the progress of recrystallization.

The force of the second phase hindering the migration of grain boundaries or dislocations in 7075 and Sc–Zr–7075 aluminum alloys can be expressed by Eqs. (2) and (3), respectively:

$$P_{Z(7075)} = P_{Z1} \quad (2)$$

$$P_{Z(\text{Sc-Zr-7075})} = P_{Z1} + P_{Z2} \quad (3)$$

The influence of the second phase particles on the grain boundary mobility can be expressed by [37]

$$V = MP_{\text{Eff}} = M_0 \exp\left(-\frac{Q}{RT}\right)(P_D - P_Z - P_C) \quad (4)$$

where  $P_{Z1}$  represents the pinning force of the second phase for grain boundary or dislocation migration in the alloy except for the  $\text{Al}_3(\text{Sc,Zr})$  phase;  $P_{Z2}$  represents the resistance of  $\text{Al}_3(\text{Sc,Zr})$  phase against the grain boundary or dislocation migration in the alloy;  $P_D$  represents the driving force for recrystallization;  $P_C$  represents the obstructive force of interface bending;  $V$  represents the interface migration speed;  $Q$  represents the activation energy;  $M_0$  represents the interface migration constant [38]. It is assumed that the remaining second phases of 7075 and Sc–Zr–7075 aluminum alloys were the same except for the  $\text{Al}_3(\text{Sc,Zr})$  phase. According to Eqs. (2)–(4), Sc–Zr–7075 aluminum alloy has a larger  $P_Z$  value and a smaller  $V$  value. Therefore, the addition of Sc and Zr effectively reduces the interface migration speed of the alloy and effectively inhibits the growth of recrystallized grain.

### 3.5 Mechanical properties

The tensile strength (UTS), yield strength (YS), and elongation (EL) of aged (120 °C, 24 h) alloys are presented in Fig. 11. Synchronous enhancements in strength and ductility were obtained in Sc–Zr–7075 aluminum alloys. The UTS, YS and EL of Sc–Zr–7075 aluminum alloy reached 696 MPa, 652 MPa and 10%, respectively. Compared to those of 7075 aluminum alloy, the UTS, YS and EL of Sc–Zr–7075 aluminum alloy increased by 21.7%, 29.6%, and 25.0%, respectively. The improvement of strength was

mainly due to grain refinement and Orowan strengthening of the secondary  $\text{Al}_3(\text{Sc,Zr})$  phase. The addition of Sc and Zr significantly increased the elongation of 7075 aluminum alloy. The reason for this can be twofold: (1) The primary  $\text{Al}_3(\text{Sc,Zr})$  phase coherent with the aluminum matrix formed during the solidification process effectively served as the nucleation core of  $\alpha(\text{Al})$  and refined the grain; (2) The secondary  $\text{Al}_3(\text{Sc,Zr})$  phase precipitated during the homogenization and subsequent solution treatment process had a strong pinning effect on the dislocations and sub-grain boundaries, preventing the growth of recrystallized grain.

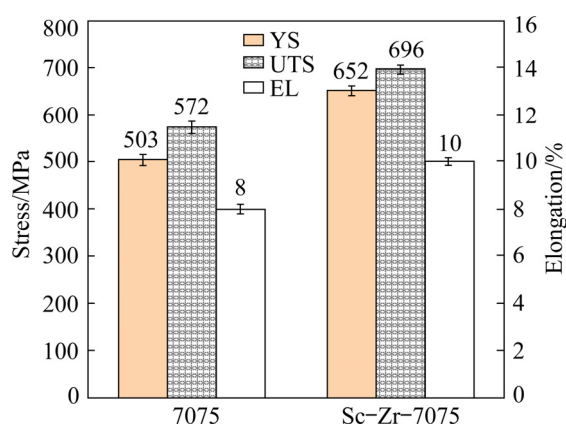


Fig. 11 Mechanical properties of 7075 and Sc-Zr-7075 aluminum alloys (T6)

## 4 Conclusions

(1) The co-addition of Sc and Zr effectively inhibited the occurrence of recrystallization of 7075 aluminum alloy. The recrystallization fraction decreased from 35% of 7075 to 22% of Sc-Zr-7075 aluminum alloy, and the corresponding substructure fraction increased from 59% to 67%.

(2) The fine and coherent  $\text{Al}_3(\text{Sc,Zr})$  phase ( $r=35$  nm,  $f=1.8\times 10^{-3}$ ) strongly hindered the migration of the dislocations and grain boundaries, preventing the formation and growth of recrystallized core of the alloy.

(3) The addition of Sc and Zr improved both the strength and elongation of 7075 aluminum alloy. The ultimate tensile strength, yield strength, and elongation of Sc-Zr-7075 aluminum alloy reached 696 MPa, 652 MPa and 10%, respectively. Compared to those of 7075 aluminum alloy, the UTS, YS and EL of Sc-Zr-7075 aluminum alloy increased by 21.7%, 29.6% and 25.0%, respectively.

## Acknowledgments

The authors are grateful for the financial supports from the National Natural Science Foundation of China (No. 51871111), the Natural Science Foundation of Shandong Province, China (No. ZR2018LE001), the Science and Technology Program of University of Ji'nan, China (Nos. XKY2036, XKY1713), and the Key Research and Development Program of Shandong Province, China (No. 2019GGX102008).

## References

- [1] CHUNG T F, YANG Y L, HUANG B M, SHI Z S, LIN J G, OHMURA T, YANG J R. Transmission electron microscopy investigation of separated nucleation and in-situ nucleation in AA7050 aluminum alloy [J]. *Acta Materialia*, 2018, 149: 377–387.
- [2] ZHANG Xue-song, CHEN Yong-jun, HU Jun-ling. Recent advances in the development of aerospace materials [J]. *Progress in Aerospace Sciences*, 2018, 97: 22–34.
- [3] SADAWY M, SAAD S, ABDEL-KARIM R. Effect of Zn/Mg ratio on cathodic protection of carbon steel using Al-Zn-Mg sacrificial anodes [J]. *Transactions of Nonferrous Metals Society of China*, 2020, 30: 2067–2078.
- [4] LI Y Y, WANG W H, HSU Y F, TRONG S. High-temperature tensile behavior and microstructural evolution of cold-rolled Al-6Mg-0.4Sc-0.13Zr alloy [J]. *Materials Science and Engineering A*, 2008, 497: 426–431.
- [5] KHENG E, IYER H R, PODSIADLO P, KAUSHIK A K, KOTOV N A, ARRUDA E M, WAAS A M. Fracture toughness of exponential layer-by-layer polyurethane/poly(acrylic acid) nanocomposite films [J]. *Engineering Fracture Mechanics*, 2010, 77: 249–256.
- [6] SHEN Chen, SUN Hui. Effects of intermediate deformation heat treatment on recrystallization structure and mechanical properties of 7050 aluminum alloy [J]. *Hot Work Technology*, 2020, 49: 122–127. (in Chinese)
- [7] DING S, KHAN S A, YANAGIMOTO J. Flow behavior and dynamic recrystallization mechanism of A5083 aluminum alloys with different initial microstructures during hot compression [J]. *Materials Science and Engineering A*, 2020, 787: 139522.
- [8] GUO Z Y, ZHAO G, CHEN X G. Effects of homogenization treatment on recrystallization behavior of 7150 aluminum sheet during post-rolling annealing [J]. *Materials Characterization*, 2016, 114: 79–87.
- [9] NES E, RYUM N, HUNDERI O. On the Zener drag [J]. *Acta Metallurgica Sinica*, 1985, 33: 11–22.
- [10] LI Lan-bo, LI Rui-di, YUAN Tie-chui, CHEN Chao, ZHANG Zhi-jian, LI Xiao-feng. Microstructures and tensile properties of a selective laser melted Al-Zn-Mg-Cu (Al7075) alloy by Si and Zr microalloying [J]. *Materials Science and Engineering A*, 2020, 787: 139492.
- [11] XIAO Quan-feng, HUANG Ji-wu, JIANG Ying-ge, JIANG Fu-qin, WU Yun-feng, XU Guo-fu. Effects of minor Sc and

- Zr additions on mechanical properties and microstructure evolution of Al–Zn–Mg–Cu alloys [J]. Transactions of Nonferrous Metals Society of China, 2020, 30: 1429–1438.
- [12] ENGLER O. On the influence of dispersoids on the particles stimulated nucleation of recrystallization in an Al–Fe–Si model alloy [J]. Materials Science Forum, 1998, 273: 483–488.
- [13] SOMERDAY M, HUMPHREYS F J. Recrystallisation behaviour of supersaturated Al–Mn alloys [J]. Materials Science Technology, 2003, 19: 20–29.
- [14] VLACH M, CIZEK J, KODETOVA V, LEIBNER M, CIESLAR M, HARCUBA P, BAJTOSOVA L, KUDRNOVA H, VLASAK T, NEUBERT V, VOLKMAR N, CERNOSKOVA E, KUTALEK P. Phase transformations in novel hot-deformed Al–Zn–Mg–Cu–Si–Mn–Fe(–Sc–Zr) alloys [J]. Materials and Design, 2020, 193: 108821.
- [15] VLACH M, CIZEK J, KODETOVA V, KEKULE T, LUKAC F, CIESLAR M, KUDRNOVA H, BAJTOSOVA L, LEIBNER M, HARCUBA P, MALEK J, NEUBERT V. Annealing effects in cast commercial aluminum Al–Mg–Zn–Cu(–Sc–Zr) alloys [J]. Metals and Materials International, 2019, 278: 1–10.
- [16] SUN N, PATTERSON B R, SUNI J P, DOHERTY R D, WEILAND H, KADOLKAR P, BLUE C A, THOMPSON G B. Effect of heating rate on recrystallization of twin roll cast aluminum [J]. Metallurgical and Materials Transactions A, 2008, 39: 165–170.
- [17] JAZAERI H, HUMPHREYS F J. The transition from discontinuous to continuous recrystallization in some aluminum alloys: II–Annealing behaviour [J]. Acta Materialia, 2004, 52: 3251–3262.
- [18] LI X Z, HANSEN V, GJONNES J, WALLEMBERG L R. HREM study and structure modeling of the  $\eta'$  phase, the hardening precipitates in commercial Al–Zn–Mg alloys [J]. Acta Materialia, 1999, 47: 2651–2659.
- [19] VLACH M, KODETOVA V, CIZEK J, LEIBNER M, KEKULE T, LUKAC F, CIESLAR M, BAJTOSOVA L, KUDRNOVA H, SIMA V, ZIKMUND S, CERNOSKOVA E, KUTALEK P, NEUBERT V. Role of small addition of Sc and Zr in clustering and precipitation phenomena induced in AA7075 [J]. Metals, 2021, 11: 1–20.
- [20] DENG Ying, YIN Zhi-min, ZHAO Kai, DUAN Jia-qi, HE Zhen-bo. Effects of Sc and Zr microalloying additions on the microstructure and mechanical properties of new Al–Zn–Mg alloys [J]. Journal of Alloys and Compounds, 2012, 530: 71–80.
- [21] LI Yun-tao, LIU Zhi-yi, XIA Qing-kun, LIU Yan-bin. Grain refinement of the Al–Cu–Mg–Ag alloy with Er and Sc additions [J]. Metallurgical and Materials Transactions A, 2007, 38: 2853–2858.
- [22] YU Kun, LI Wen-xian, LI Song-ru, ZHAO Jun. Mechanical properties and microstructure of aluminum alloy 2618 with  $Al_3(Sc,Zr)$  phases [J]. Materials Science and Engineering A, 2004, 368: 88–93.
- [23] TENG G B, LIU C Y, MA Z Y, ZHOU W B, WEI L L, CHEN Y, LI J, MO Y F. Effects of minor Sc addition on the microstructure and mechanical properties of 7055 Al alloy during aging [J]. Materials Science and Engineering A, 2018, 713: 61–66.
- [24] LI Bo, PAN Qing-lin, HUAN Xing, YIN Zhi-min. Microstructures and properties of Al–Zn–Mg–Mn alloy with trace amounts of Sc and Zr [J]. Materials Science and Engineering A, 2014, 616: 219–228.
- [25] BURANOVA Y, KULITSKIY V, PETERLECHNER M, MOGUCHEVA A, KAIBYSHEV R, DIVINSKI S V, WILDE G.  $Al_3(Sc,Zr)$ -based precipitates in Al–Mg alloy: Effect of severe deformation [J]. Acta Materialia, 2017, 124: 210–224.
- [26] DENG Ying, PENG Bing, XU Guo-fu, PAN Qing-lin, YIN Zhi-min, YE Rui, WANG Ying-jun, LU Li-ying. Effects of Sc and Zr on mechanical property and microstructure of tungsten inert gas and friction stir welded aerospace high strength Al–Zn–Mg alloys [J]. Materials Science and Engineering A, 2015, 639: 500–513.
- [27] KODETOVA V, VLACH M, KUDRNOVA H, MALEK J, CIESLAR M, BAJTOSOVA L, KEKULE T, HARCUBA P, LUKAC F, LEIBNER M. Phase transformations in commercial cold rolled Al–Zn–Mg–Cu alloys with Sc and Zr addition [J]. Journal of Thermal Analysis and Calorimetry, 2020, 237: 1–12.
- [28] KODETOVA V, VLACH M, KUDRNOVA H, LEIBNER M, MALEK J, CIESLAR M, BAJTOSOVA L, HARCUBA P, NEUBERT V. Annealing effects in commercial aluminum hot-rolled 7075(–Sc–Zr) alloys [J]. Journal of Thermal Analysis and Calorimetry, 2020, 142: 1613–1623.
- [29] GUAN Ren-guo, SHEN Yong-feng, ZHAO Zhan-yong, WANG Xiang. A high-strength, ductile Al–0.35Sc–0.2Zr alloy with good electrical conductivity strengthened by coherent nanosized-precipitates [J]. Journal of Materials Science and Technology, 2017, 33: 215–223.
- [30] RANGANATHA R, KUMAR V A, NANDI V S, BHAT R, MURALIDHARA B. Multi-stage heat treatment of aluminum alloy AA7049 [J]. Transactions of Nonferrous Metals Society of China, 2013, 23: 1570–1575.
- [31] PENG Xiao-yan, LI Yao, LIANG Xiao-peng, GUO Qi, XU Guo-fu, PENG Yong-yi, YIN Zhi-min. Precipitate behavior and mechanical properties of enhanced solution treated Al–Zn–Mg–Cu alloy during non-isothermal aging [J]. Journal of Alloys and Compounds, 2018, 735: 964–974.
- [32] LIN Y, PENG X B, JIANG Y Q, SHUAI C J. Effects of creep-aging parameters on aging precipitates of a two-stage creep-aged Al–Zn–Mg–Cu alloy under the extra compressive stress [J]. Journal of Alloys and Compounds, 2018, 743: 448–455.
- [33] HE Yong-dong, ZHANG Xin-ming. Mechanism on annealing recrystallization of Al–Zn–Mg–Cu–Sc alloy [J]. Rare Metal Materials and Engineering, 2009, 38: 1945–1949. (in Chinese)
- [34] PENG Ying-hao, LIU Chong-yu, WEI Li-li, JIANG Hong-Jie, GE Zhen-jiang. Quench sensitivity and microstructures of high-Zn-content Al–Zn–Mg–Cu alloys with different Cu contents and Sc addition [J]. Transactions of Nonferrous Metals Society of China, 2021, 31: 24–35.
- [35] DILLAMORE I L, KATOH H. The mechanisms of recrystallization in cubic metals with particular reference to their orientation-dependence [J]. Metal Science, 1974, 8: 73–83.
- [36] LIN H P, DELPHIC C, KUO J C. Grain boundary evolution of cold-rolled FePd alloy during recrystallization at

- disordering temperature [J]. *Materials*, 2015, 8: 3254–3267.
- [37] HUMPHREYS F J, HATHERLY M. Recrystallization and related annealing phenomena [M]. Kidlington: Elsevier, 2004. (in Chinese)
- [38] HUNG K, MARTHINSEN K, ZHAO Q L, LOGE R E. The

double-edge effect of second-phase particles on the recrystallization behaviour and associated mechanical properties of metallic materials [J]. *Progress in Materials Science*, 2017, 92: 284–359.

## Sc 和 Zr 对 7075 铝合金再结晶行为的影响

冷金凤<sup>1</sup>, 任丙辉<sup>1</sup>, 周庆波<sup>2</sup>, 赵纪薇<sup>1</sup>

1. 济南大学 材料科学与工程学院, 济南 250022;
2. 山东中铝烯碳材料有限公司, 济南 250031

**摘 要:** 研究通过铸造法制备的含  $\text{Al}_3(\text{Sc,Zr})$  相的 7075 铝合金静态再结晶行为和再结晶行为与力学性能的关系。Sc 和 Zr 复合添加使 Sc-Zr-7075 铝合金保留挤压变形过程中形成的大部分纤维组织及高密度位错, 导致合金的再结晶转变量由 35% 降低至 22%, 相应的亚结构保持量由 59% 升高至 67%。Sc 和 Zr 有效抑制 7075 铝合金再结晶行为, 这主要归因于细小弥散 ( $r=35\text{ nm}$ ,  $f_v=1.8\times 10^{-3}$ ) 的  $\text{Al}_3(\text{Sc,Zr})$  相对位错和亚晶界具有强烈的钉扎作用, 阻碍位错重新排列成亚晶界及随后发展成大角度晶界, 进而阻碍合金再结晶核心的形成和长大。

**关键词:** 7075 铝合金;  $\text{Al}_3(\text{Sc,Zr})$  相; 再结晶; 力学性能

(Edited by Bing YANG)